Inorg. Chem. **2003**, *42*, 128–139

Self-Assembled Supramolecular M_9 (Mn(II), Fe(III), Zn(II)), M_5 (Fe(III)), and $[M_3]_2$ (Pb(II)) Complexes: Structural, Magnetic, and Mössbauer Properties

Laurence K. Thompson,*,† Liang Zhao,† Zhiqiang Xu,† David O. Miller,† and William M. Reiff*,‡

Department of Chemistry, Memorial University of Newfoundland, St. John's, Newfoundland A1B 3X7, Canada, and Department of Chemistry, Northeastern University, Boston, Massachusetts 02114

Received July 19, 2002

The tritopic ligand 2poap self-assembles in the presence of $Zn(NO_3)_2$ and $Fe(NO_3)_3$ to form homoleptic [3 × 3] nonanuclear M_9 (M = Zn(II), Fe(III)) square grid structures and with $Pb(ClO_4)_2$ to form a dimerized linear trinuclear $[Pb_3]_2$ structure. Cl2poap and Cl2poapz form self-assembled homoleptic [3 × 3] $Mn(II)_9$ square grids with $Mn(ClO_4)_2$ and $Mn(NO_3)_2$, respectively, but an unusual incompletely metalated $Fe(III)_5$ square grid is formed on reaction of Cl2poap with $Fe(ClO_4)_3$. X-ray structures are reported for $[Mn_9(Cl2poap\text{-}2H)_6](ClO_4)_6\cdot 10H_2O$ (**3**), $[Mn_9(Cl2poapz\text{-}2H)_6](NO_3)_6\cdot 22H_2O$ (**4**), $[Zn_9(2poap\text{-}2H)_3(2poap\text{-}H)_3](NO_3)_9\cdot 24H_2O$ (**5**), $[Pb_3(2poap\text{-}2H)(ClO_4)_4]_2.8H_2O$ (**6**), and $[Fe_5(Cl2poap\text{-}H)_6](ClO_4)_9\cdot 34.5H_2O$ (**7**). Compound **3** crystallized in the monoclinic system, space group $P\bar{1}$, with a = 18.179(1) Å, b = 18.857(1) Å, c = 25.871(2) Å, α = 70.506(2)°, β = 86.440(1)°, γ = 75.175(2)°, and z = 2. Compound **4** crystallized in the monoclinic system, space group $P\bar{1}$, with a = 16.900(2) Å, b = 20.02393) Å, c = 25.663() Å, α = 84.743(3)°, β = 84.885(2)°, γ = 67.081(2)°, and z = 2. Compound **5** crystallized in the monoclinic system, space group $P\bar{1}$, with a = 18.482(1) Å, b = 18.774(1) Å, c = 28.112(2) Å, α = 104.020(1)°, β = 97.791(1)°, γ = 117.036(1)°, and z = 2. Compound **6** crystallized in the monoclinic system, space group $P\bar{1}$, with a = 10.0513(6) Å, b = 11.0958(6) Å, c = 17.334(1) Å, α = 100.932(1)°, β = 100.387(1)°, γ = 94.565(1)°, and z = 2. Compound **7** crystallized in the monoclinic system, space group $P\bar{1}$, with a = 19.164(1) Å, b = 19.587(2) Å, c = 26.673(2) Å, α = 76.430(2)°, β = 78.834(2)°, γ = 64.973(1)°, and z = 2. Compound **3** exhibits intramolecular antiferromagnetic exchange within the nonanuclear $[Mn_9(\mu\text{-}O)_{12}]$ grid structure (J = –4.6 cm^{-1}), while the analogous nonanuclear complex $[Fe_9(2poap\text{-}2H)_6](NO_3)_{15}\cdot 18H_2O$ **(8)** is dominated by intramolecular antiferromagnetic coupling at high temperatures but exhibits a low-temperature feature indicative of additional ferromagnetic interactions. The isolated pentanuclear Fe_5 [4 + 1] square grid in **7**, with distant Fe–Fe bridging, exhibits very weak antiferromagnetic coupling (J = –0.2 cm^{-1}). Mössbauer spectroscopy data are consistent with high-spin $Fe(III)_9$ and $Fe(III)_5$ structures.

Introduction

The spontaneous assembly of metal ion centers into homoleptic grids or clusters offers a particularly attractive method for the production of nanosized, supramolecular aggregates whose properties will be a direct consequence of the positioning and identity of the coordination pockets within the ligand and the ability of the metal ion to read these sites in terms of its own coordination algorithms. With the appropriate choice of donors, bridging groups, and paramagnetic metal ions, magnetic coupling can be fine-tuned so that a desired supramolecular magnetic property may result. In the design of nanoscale materials, grid structures are of special interest because a two-dimensional, precise gridlike configuration of the metal centers suggests applications in information storage and processing technology. Moreover, depending on the packing, such assemblages of grids have the potential to exhibit either long-range order or single molecule magnetic behavior.

Linear polytopic ligands based on pyridazine bridging subunits have produced molecular [2 × 2] $Cu(I)_4$[1] and [3 ×

* Authors to whom correspondence should be addressed. (L.K.T.) fax: 709-737-3702; e-mail: lthomp@morgan.ucs.mun.ca. (W.M.R.) fax: 617-373-8795; e-mail: w.reiff@neu.edu.

† Memorial University of Newfoundland.

‡ Northeastern University.

10.1021/ic020468y CCC: $25.00
Published on Web 12/07/2002

3] $Ag(I)_9$[2] grids, by a strict self-assembly process, with the metal ions fitting neatly into the tetrahedral pockets created by the assembly of pairs of ligands, which provide N_2-donor groupings above and below the planar arrangement of metal centers. Mixing similar ditopic and tritopic ligands can lead to a mixed [2 × 3] rectangular Ag_6 grid, along with small amounts of homoligand Ag_4 and Ag_9 grid complexes.[3] Examples of [2 × 2] homo- and heterometallic grids[4,5] of six-coordinate metal ions have been produced with ligands based on pyrimidine bridging subunits, where the donor groupings arise from the assembly of pairs of ligands that combine N_3 donor pockets. With Co(II) and Ni(II) salts, magnetically coupled [2 × 2] grids form with such ligands, exhibiting intramolecular antiferromagnetic exchange,[6,7] despite long distances between metal centers (6.5 Å for Co). A recent report, based on NMR and ES mass spectrometry, indicates that with appropriate extension of these pyrimidine-based ligands [4 × 4] Pb_{16} square grids can also be produced.[8]

Linear polytopic ligands that are built around single atom bridging subunits stand a better chance of producing magnetically coupled grids with significant intramolecular exchange interactions and potentially useful molecular magnetic properties. A homoleptic tetranuclear $Cu_4(\mu\text{-}O)_4$ phenoxide bridged [2 × 2] square grid formed from a ditopic phenoxide-based ligand exhibits very weak antiferromagnetic coupling, in agreement with the nominally orthogonal Cu−O−Cu bridging arrangement.[9] A homoleptic square $Co(II)_4$ self-assembled grid with the ligand tetra(2-pyridyl)thiocarbazone has a $Co_4(\mu\text{-}S)_4$ core, but no magnetic properties were reported.[10] Flexible linear polytopic ligands based on combinations of diazine (N−N) and alkoxo subunits (e.g., poap and poapz (Scheme 1)), have the potential for a wide variety of coordination modes but mostly produce self-assembled, nonhomoleptic [2 × 2] square, tetranuclear alkoxo-bridged $M_4(\mu\text{-}O)_4$ grids (M = Cu(II), Ni(II), Co(II), Mn(II)) with potentially coordinating anions.[11,12] The copper systems exhibit intramolecular ferromagnetic coupling, associated with an orthogonal arrangement of copper magnetic orbitals

Scheme 1

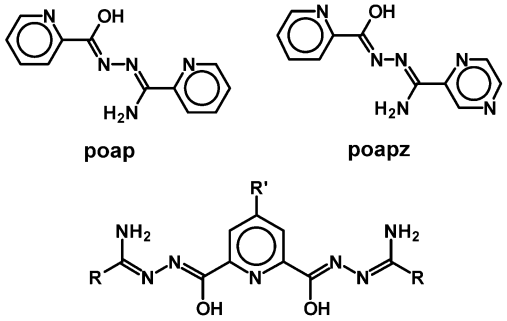

within the grid framework, while in the other cases antiferromagnetic coupling is observed. These ligands appear to take part in an anion-dependent self-assembly process with octahedral metal centers, and homoleptic, pentanuclear alkoxo-bridged trigonal-bipyramidal clusters form with non-coordinating anions (e.g., ClO_4^-) with Mn(II), Co(II), and Zn(II) salts.[13a,b] Intramolecular antiferromagnetic coupling is observed for the Mn(II) and Co(II) complexes. Anion templating assembly has been implicated in the formation of the square magnetically uncoupled grid $[Ni_4(bptz)_4(CH_3CN)_8](BF_4)_8$ (bptz = 3,6-bis(2-pyridyl)tetrazine),[14] which has well-separated metal centers but appears not to be necessary for the assembly of the corresponding zinc complex $[Zn_4(bptz)_4(CH_3CN)_8(H_2O)_4](ClO_4)_8$.[15]

Extension of the alkoxy-diazine ligands poap and poapz (Scheme 1) to effectively double the alkoxo-bridging fragment can be achieved by using a 2,6-disubstituted pyridine central unit (e.g., 2poap, Cl2poap, 2poapz, etc.; Scheme 1), which results in the formation of unique nonanuclear [3 × 3] $[M_9(\mu\text{-}O_{12})]$ paramagnetic grids in $[Mn_9(2poap\text{-}2H)_6](ClO_4)_6\cdot 18H_2O$ (**1**)[16] and $[Cu_9(2poap\text{-}H)_6](NO_3)_{12}\cdot 9H_2O$ (**2**)[17,18] by strict self-assembly processes with Mn(II) and Cu(II) salts, respectively. The Mn_9 system exhibits intramolecular antiferromagnetic coupling, with a $S = 5/2$ ground state,[19] while for the Cu_9 complex ferromagnetic exchange is observed with a $S = 7/2$ ground state.[17,18] The present study reports further details on two new Mn(II) systems, a similar magnetically coupled Fe(III)$_9$ complex $[Fe_9(2poap\text{-}2H)_6](NO_3)_{15}\cdot 18H_2O$

(1) Youinou, M.-T.; Rahmouni, N.; Fischer, J.; Osborn, J. A. *Angew. Chem., Int. Ed. Engl.* **1992**, *31*, 733.
(2) Baxter, P. N. W.; Lehn, J.-M.; Fischer, J.; Youinou, M.-T. *Angew. Chem., Int. Ed. Engl.* **1994**, *33*, 2284.
(3) Baxter, P. N. W.; Lehn, J.-M.; Kneisel, B. O.; Fenske, D. *Angew. Chem., Int. Ed. Engl.* **1997**, *36*, 1978.
(4) Hanan, G. S.; Volkmer, D.; Ulrich, S. S.; Lehn, J.-M.; Baum, G.; Fenske, D. *Angew. Chem., Int. Ed. Engl.* **1997**, *36*, 1842.
(5) Bassani, D. M.; Lehn, J.-M.; Fromm, K.; Fenske, D. *Angew. Chem., Int. Ed.* **1998**, *37*, 2364.
(6) Waldmann, O.; Hassmann, J.; Müller, P.; Hanan, G. S.; Volkmer, D.; Schubert, U. S.; Lehn, J.-M. *Phys. Rev. Lett.* **1997**, *78*, 3390.
(7) Waldmann, O.; Hassmann, J.; Müller, P.; Hanan, G. S.; Volkmer, D.; Schubert, U. S.; Lehn, J.-M. *Phys. Rev. B* **1998**, *58*, 3277.
(8) Garcia, A. M.; Romero-Salguero, F. J.; Bassani, D. M.; Lehn, J.-M.; Baum, G.; Fenske, D. *Chem.—Eur. J.* **1999**, *5*, 1803.
(9) Rojo, J.; Lehn, J.-M.; Baum, G.; Fenske, D.; Waldmann, O.; Müller. P. *Eur. J. Inorg. Chem.* **1999**, 517.
(10) Duan, C.-y.; Liu, Z.-h.; You, X.-z.; Xue, F.; Mak, T. W. C. *J. Chem. Soc., Chem. Commun.* **1997**, 381.
(11) Matthews, C. J.; Avery, K.; Xu, Z.; Thompson, L. K.; Zhao, L.; Miller, D. O.; Biradha, K.; Poirier, K.; Zaworotko, M. J.; Wilson, C.; Goeta, A. E.; Howard, J. A. K. *Inorg. Chem.* **1999**, *38*, 5266.
(12) Thompson, L. K.; Matthews, C. J.; Zhao, L.; Xu, Z.; Miller, D. O.; Wilson, C.; Leech, M. A.; Howard, J. A. K.; Heath, S. L.; Whittaker, A. G.; Winpenny, R. E. P. *J. Solid State Chem.* **2001**, *159*, 308.
(13) (a) Matthews, C. J.; Xu, Z.; Mandal, S. K.; Thompson, L. K.; Biradha, K.; Poirier, K.; Zaworotko, M. J. *J. Chem. Soc., Chem. Commun.* **1999**, 347. (b) Matthews, C. J.; Thompson, L. K.; Parsons, S. R.; Xu, Z.; Miller, D. O.; Heath, S. L. *Inorg. Chem.* **2001**, *40*, 4448.
(14) Campos-Fernández, C. S.; Clérac, R.; Dunbar, K. R. *Angew. Chem., Int. Ed.* **1999**, *38*, 3477.
(15) Bu, X.-H.; Morishita, H.; Tanaka, K.; Biradha, K.; Furusho, S.; Shinoya, M. *J. Chem. Soc., Chem. Commun.* **2000**, 971.
(16) Zhao, L.; Matthews, C. J.; Thompson, L. K.; Heath, S. L. *J. Chem. Soc., Chem. Commun.* **2000**, 265.
(17) Zhao, L.; Xu, Z.; Thompson, L. K.; Heath, S. L.; Miller, D. O.; Ohba, M. *Angew. Chem., Int. Ed.* **2000**, *39*, 3114.
(18) Waldmann, O.; Koch, R.; Schromm, S.; Müller, P.; Zhao, L.; Thompson, L. K. *Chem. Phys. Lett.* **2000**, *332*, 73.
(19) Waldmann, O.; Zhao, L.; Thompson, L. K. *Phys. Rev. Lett.* **2002**, *88*, 066401.

(**8**) (brief details of which have already been reported),[20] and $Zn(II)_9$, $(Pb(II)_3)_2$, and $Fe(III)_5$ derivatives with the ligands 2poap, Cl2poap, and Cl2poapz. Structures, magnetic properties, and Mössbauer data are discussed.

Experimental Section

Physical Measurements. Infrared spectra were recorded as Nujol mulls using a Mattson Polaris FT-IR instrument. UV−vis spectra were recorded in the solid state (mull transmittance) using a Cary 5E spectrometer. MALDI/TOF mass spectra were obtained with an Applied Biosystems Voyager System 2026 using a CHCA calibration matrix. Samples were dissolved in acetonitrile. Microanalyses were carried out by Canadian Microanalytical Service, Delta, Canada. Hydrogen analyses for **5** and **7** are somewhat lower than anticipated, but other elemental analyses are consistent with the proposed analytical formulas. Such a situation occurs occasionally with systems of this sort. Variable temperature magnetic data (2−300 K) were obtained using a Quantum Design MPMS5S SQUID magnetometer with field strengths in the range of 0.1−5.0 T. Samples were prepared in gelatin capsules or aluminum pans and mounted inside straws for attachment to the sample transport rod. Background corrections for the sample holder assembly and diamagnetic components of the complexes were applied.

The Mössbauer spectra were determined using a conventional constant acceleration spectrometer operated in a multichannel scaling mode. The γ ray source consisted of a fresh 120 mCi of Co^{57} in a rhodium metal matrix that was maintained at ambient temperature. The spectrometer was calibrated using a 6-μm-thick natural abundance iron foil. Isomer shifts are reported relative to the center of the magnetic hyperfine pattern of the latter foil taken as zero velocity. The line widths of the innermost pair of $\Delta M_I = \pm 1$ transitions of the latter Zeeman pattern were reproducibly determined to be 0.214 mm/s. Sample temperature variation was achieved using a standard exchange gas liquid helium cryostat (Cryo Industries of America, Inc.) with temperature measurement and control based on silicon diode thermometry in conjunction with a 10 μA excitation source (Lakeshore Cryotronics, Inc). The spectra were initially fitted to unconstrained Lorentzians using the program ORIGIN (Microcal Software, Inc.)

Synthesis of the Ligands and Complexes. 2poap. 2poap was synthesized as reported previously.[16,17] Cl2poap was synthesized in the same manner starting from 4-chloro-2,6-pyridine dicarboxylic acid. Cl2poapz was synthesized in the same manner using the imino ester of 2-cyanopyrazine in the final step. Satisfactory elemental analyses were obtained for the ligands (Scheme 1).

$[Mn_9(Cl2poap\text{-}2H)_6](ClO_4)_6\cdot 10H_2O$ (3). Cl2poap (0.438 g, 1.0 mmol) was suspended in a hot solution of $Mn(ClO_4)_2\cdot 6H_2O$ (0.73 g, 2.0 mmol) in methanol (20 mL) and MeCN (10 mL). A clean red solution was formed in a few minutes, which was filtered and allowed to stand at room temperature for a few days. Orange-red crystals formed (yield: 88.4%). Anal. Calcd $Mn_9(C_{19}H_{15}N_9O_2Cl)_6(ClO_4)_6(H_2O)_{10}$: C, 35.18; H, 2.85; N, 19.43. Found: C, 35.04; H, 2.85; N, 19.29. IR (Nujol mull, cm^{-1}): 3575, 3457, 3350, 3150 (νH_2O, NH), 1657 ($\nu C{=}N$), 1096 (ClO_4^-). MALDI/TOFMS: 3103.3 (M^+, $C_{114}H_{78}N_{54}O_{12}Cl_6Mn_9$), 3203.6 ($M(HClO_4)$), 3305.5 $(M(HClO_4)_2)$.

$[Mn_9(Cl2poapz\text{-}2H)_6](NO_3)_6\cdot 22H_2O$ (4) was synthesized in a manner similar to **3** using Cl2poapz and $Mn(NO_3)_2\cdot 6H_2O$ and obtained as red-brown prismatic crystals (yield: 83%). Anal. Calcd $Mn_9(C_{17}H_{12}N_{11}O_2Cl)_6(NO_3)_6(H_2O)_{22}$: C, 31.49; H, 3.00; N, 25.93. Found: C, 31.39; H, 2.44; N, 25.71. IR (Nujol mull, cm^{-1}): 3450 (br) (νH_2O, NH), 1731 ($\nu_1 + \nu_4$ NO_3), 1657 ($\nu C{=}N$). MALDI/TOF MS: 3113.9 (M^+, $C_{102}H_{72}N_{66}O_{12}Cl_2Mn_9$).

$[Zn_9(2poap\text{-}2H)_3(2poap\text{-}H)_3](NO_3)_9\cdot 24H_2O$ (5). 2poap (0.405 g, 1.0 mmol) was suspended in a hot solution of $Zn(NO_3)_2\cdot 6H_2O$ (2.3 g, 5.0 mmol) in 10 mL of deionized water. A total of 5 mL of methanol was added to form a clear yellow-orange solution after a few minutes. The solution was filtered and allowed to stand at room temperature for a few days. Yellow-orange crystals, suitable for X-ray analysis, formed (yield: 80%). Anal. Calcd $[Zn_9(C_{19}H_{15}N_9O_2)_3(C_{19}H_{16}N_9O_2)_3](NO_3)_9\cdot 24H_2O$: C, 34.31; H, 3.56; N, 22.11. Found: C, 34.06; H, 2.46; N, 22.46. IR (Nujol mull, cm^{-1}): 3592 (νH_2O), 3442, 3175 (νNH), 1639 ($\nu C{=}N$) and 1019 (ν py).

$[Pb_3(2poap\text{-}2H)(ClO_4)_4]_2\cdot 8H_2O$ (6). 2poap (0.405 g, 1.0 mmol) was suspended in a hot solution of $Pb(ClO_4)_2\cdot 3H_2O$ (2.3 g, 5.0 mmol) in 10 mL of deionized water. A total of 5 mL of methanol was added with the formation of a clear yellow-orange solution after a few minutes. The solution was filtered and allowed to stand at room temperature for a few days. Yellow crystals, suitable for X-ray analysis, formed (yield: 80%). Anal. Calcd $[Pb_3(C_{19}H_{15}N_9O_2)(ClO_4)_4]_2\cdot 8H_2O$: C, 15.29; H, 1.55; N, 8.44. Found: C, 15.18; H, 1.51; N, 8.31. IR (Nujol mull, cm^{-1}): 3592 (νH_2O), 3368, 3165 (νNH), 1657 ($\nu C{=}N$), 1080, 625 (νClO_4^-).

$[Fe_5(Cl2poap\text{-}H)_6](ClO_4)_9\cdot 34.5H_2O$ (7). A total of 0.438 g of Cl2poap (1.0 mmol) was suspended in a hot solution of $Fe(ClO_4)_3\cdot 6H_2O$ (0.93 g, 2.0 mmol) in methanol (20 mL) and MeCN (10 mL). A clean deep green solution was formed in a few minutes. The solution was filtered and allowed to stand at room temperature for a few days. Dark green crystals formed (yield: 87.0%). Found: C, 30.71; H, 2.57; N, 17.02. $[(C_{19}H_{15}N_9O_2Cl)_6Fe_5](ClO_4)_9(H_2O)_{34.5}$: requires C, 31.00; H, 3.63; N, 17.12. IR (Nujol mull, cm^{-1}): 3560, 3465, 3345, 3155 (νH_2O, NH), 1660 ($\nu C{=}N$), and 1095 (νClO_4^-). Adjusting the pH to ∼5−6 in the solution using either triethylamine or ammonium hydroxide resulted in the formation of the same Fe_5 derivative, with no evidence for the formation of a Fe_9 complex.

$[Fe_9(2poap\text{-}2H)_6](NO_3)_{15}\cdot 18H_2O$ (8). 2poap (0.405 g, 1.0 mmol) was suspended in a hot solution of $Fe(NO_3)_3\cdot 9H_2O$ (2.3 g, 5.7 mmol) in 10 mL of deionized water. A dark solution formed after a few minutes. The solution was filtered and allowed to stand at room temperature for a few days. Dark, almost black crystals formed (yield: 0.58 g, 84%). Several attempts to get suitable X-ray diffraction data failed because of crystal instability, even in cases where the crystals were kept under mother liquor prior to mounting quickly on the goniometer. Anal. Calcd $[Fe_9(C_{19}H_{15}N_9O_2)_6](NO_3)_{15}\cdot 18H_2O$: C, 32.87; H, 3.05; N, 23.20. Found: C, 32.84; H, 2.66; N, 23.08. IR (Nujol mull, cm^{-1}): 1680, 1655 ($\nu C{=}N$), 1014 (νpy). UV−vis (Nujol mull, nm): 916.

Safety Note. Perchlorate complexes are potentially explosive and should be handled in small quantities. No problems with the current complexes have been encountered so far.

Crystallographic Data and Refinement of the Structures. The diffraction intensities of an orange-red prismatic crystal of **3** were collected with graphite-monochromatized Mo Kα X-radiation (rotating anode generator) using a Bruker P4/CCD diffractometer at 193(1) K to a maximum 2θ value of 52.8°. The data were corrected for Lorentz and polarization effects. The structure was solved by direct methods.[21,22] All atoms except hydrogens were refined anisotropically. Hydrogen atoms were placed in calculated positions with isotropic thermal parameters set to 20% greater than

(20) Zhao, L.; Xu, Z.; Thompson, L. K.; Miller, D. O. *Polyhedron* **2001**, *20*, 1359.

(21) (a) Sheldrick, G. M. *SHELX97*; University of Göttingen: Göttingen, Germany, 1997. (b) *SIR97*: Altomare, A.; Cascarano, M.; Giacovazzo, C.; Guagliardi, A. *J. Appl. Cryst.* **1993**, *26*, 343.

Table 1. Summary of Crystallographic Data for $[Mn_9(Cl2poap\text{-}2H)_6](ClO_4)_6\cdot 10H_2O$ (**3**), $[Mn_9(Cl2poapz\text{-}2H)_6](NO_3)_6\cdot 22H_2O$ (**4**), $[Zn_9(2poap\text{-}2H)_3(2poap\text{-}H)_3](NO_3)_9\cdot 24H_2O$ (**5**), $[Pb_3(2poap\text{-}2H)(ClO_4)_4]_2\cdot 8H_2O$ (**6**), and $[Fe_5(Cl2poap\text{-}H)_6](ClO_4)_9\cdot 34.5H_2O$ (**7**)

	3	**4**	**5**	**6**	**7**
empirical form.	$C_{121}H_{113}N_{56}O_{44.5}Mn_9Cl_{12}$	$C_{102}H_{87}N_{70}O_{31.5}Cl_6Mn_9$	$C_{114}H_{132}N_{60}O_{49}Zn_9$	$C_{19}H_{26}N_9O_{23.5}Cl_4Pb_3$	$C_{118}H_{122}N_{56}O_{64}Cl_5Fe_5$
fw	3983.45	3502.42	3715.09	1519.87	4159.63
space group	$P\bar{1}$ (No. 2)	$P\bar{1}$ (No. 2)	$P\bar{1}1$ (No. 2)	$P\bar{1}$ (No. 2)	$P\bar{1}$
a (Å)	18.179(1)	16.900(2)	18.482(1)	10.0513(6)	19.164(1)
b (Å)	18.857(1)	20.023(3)	18.774(1)	11.0958(6)	19.587(2)
c (Å)	25.871(2)	25.66393)	28.112(2)	17.334(1)	26.673(2)
α (deg)	70.506(2)	84.743(3)	104.020(1)	100.932(1)	76.430(2)
β (deg)	86.440(1)	84.885(2)	97.791(1)	100.387(1)	78.834(2)
γ (deg)	75.175(2)	67.081(2)	117.036(1)	94.565(1)	64.973(1)
V (Å^3)	8079(1)	7951(2)	8081.6(9)	1854.0(2)	8768(1)
ρ_{calcd} (g cm^{-3})	1.637	1.464	1.527	2.722	1.575
Z	2	2	2	2	2
μ (mm^{-1})	0.973	0.877	1.409	14.02	7.34 cm^{-1}
λ (Å)	0.71073	0.71073	0.71073	0.71073	0.71073
T (K)	193(1)	193(1)	193(1)	193(1)	193(1)
R1[a]	0.072	0.112	0.110	0.036	0.114
wR2	0.253	0.393	0.376	0.098	0.366

[a] $R1 = \sum[|F_o| - |F_c|]/\sum|F_o|$, $wR2 = [\sum[w(|F_o|^2 - |F_c|^2)^2]/\sum[w(|F_o|^2)^2]]^{1/2}$.

their bonded partners and were not refined. Neutral atom scattering factors[23] and anomalous-dispersion terms[24,25] were taken from the usual sources. All other calculations were performed with the teXsan[26] crystallographic software package using a PC computer. Crystal data collection and structure refinement for **4** (red-brown prisms), **5** (yellow-orange prisms)**, 6** (yellow prisms), and **7** (dark green prisms) were carried out in a similar manner using Mo Kα radiation. Abbreviated crystal data for **3**−**7** are given in Table 1.

Refinements for **4, 5**, and **7** were hampered by weak data sets, lattice disorder effects, the presence of an abundance of disordered water molecules, and in particular with **4** and **5** the difficulty of identifying all of the anionic nitrate groups indicated by the elemental analysis on the bulk sample. Compound **7** contained loose perchlorate anions and a significant amount of disordered water. While the modeling of the ligands and the polymetallic cationic grid structure proceeded smoothly, the final refinement values are high because of the inferior quality of the data. The details presented are the best obtained from the current data sets, which were collected at low temperature on a rotating anode instrument equipped with a CCD detector. It is unlikely that improved refinements would be obtained with data sets from other crystalline samples. The difficulty in refining these structures is associated in part with poor crystal quality, very large cells, lattice disorder effects, large numbers of lattice-trapped solvent molecules, and as a result crystal instability. Typically, crystals must be stored under mother liquor prior to data collection and require immediate freezing once removed from the mother liquor, otherwise crystal decomposition occurs. In the case of **8,** despite our best efforts, crystal decomposition occurred even when the crystals were frozen quickly. Variation of solvent conditions, and the anion used, has so far not helped.

(22) Beurskens, P. T.; Admiraal, G.; Beurskens, G.; Bosman, W. P.; de Gelder, R.; Israel, R.; Smits, J. M. M. *DIRDIF94 Program System*; Technical Report of the Crystallography Laboratory, University of Nijmegen: The Netherlands, 1994.

(23) Cromer, D. T.; Waber, J. T. *International Tables for X-ray Crystallography*; The Kynoch Press: Birmingham, England, 1974; Vol. IV, Table 2.2 A.

(24) Ibers, J. A.; Hamilton, W. C. *Acta Crystallogr*. **1964**, *17*, 781.

(25) Creagh, D. C.; McAuley, W. J. *International Tables for Crystallography*; Wilson, A. J. C., Ed.; Kluwer Academic Publishers: Boston, 1992; Vol. C, Table 4.2.6.8, pp 219−222.

(26) *teXsan for Windows, Crystal Structure Analysis Package*; Molecular Structure Corporation: Houston, TX, 1997.

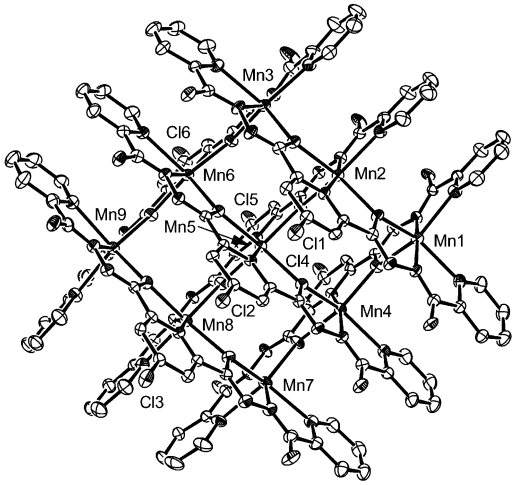

Figure 1. Structural representation of the cation in $[Mn_9(Cl2poap\text{-}2H)_6](ClO_4)_6\cdot 10H_2O$ (**3**).

Results and Discussion

Structures. $[Mn_9(Cl2poap\text{-}2H)_6](ClO_4)_6\cdot 10H_2O$ (3). The molecular structure of the nonanuclear cation in **3** is illustrated in Figure 1, and selected bond lengths and angles are listed in Table 2. The structure consists of a self-assembled homoleptic $[M_9(\mu\text{-}O)_{12}]$, [3 × 3] grid of nine pseudo-octahedral manganese(II) ions arranged in a roughly planar square array, with each metal center connected to its immediate neighbors by alkoxide bridges. The structure resembles closely that reported for $[Mn_9(2poap\text{-}2H)](ClO_4)_6\cdot 18H_2O$ (**1**).[16] Mn−Mn separations in the outer ring of eight metal centers fall in the range of 3.88−4.06 Å (average 3.97 Å), while distances from the central manganese to its immediate neighbors fall in the range of 3.94−4.03 Å (average 3.99 Å). Mn−O−Mn angles fall in the range of 126.4−130.7°. Each manganese ion occupies a pseudo-octahedral hole in the grid structure generated by the associated assembly of the six parallel ligands arranged in two groups of three above and below the metal plane. The arrangement leads to three different types of six-coordinate Mn(II) ions: *cis*-MnN_4O_2 at the corners, *mer*-MnN_3O_3 along

Table 2. Selected Interatomic Distances (Å) and Angles (deg) for Complexes **3**−**7**

		3	
Mn(5)−N(14)	2.190(5)	Mn(5)−N(41)	2.175(5)
Mn(5)−O(3)	2.196(4)	Mn(5)−O(4)	2.224(4)
Mn(5)−O(9)	2.208(4)	Mn(5)−O(10)	2.262(4)
Mn−O	2.148(4)−2.271(4)	Mn−N	2.130(5)−2.419(6)
Mn−O−Mn (ring)	126.40(19)−130.51((19)		
Mn−O−Mn (center)	127.37(18)−130.68(18)		
		4	
Mn(5)−N(17)	2.155(8)	Mn(5)−O(9)	2.177(6)
Mn(5)−N(50)	2.196(8)	Mn(5)−O(4)	2.211(6)
Mn(5)−O(3)	2.211(6)	Mn(5)−O(10)	2.225(7)
Mn−O	2.131(7)−2.225(7)	Mn−N	2.108(12)−2.422(9)
Mn−O−Mn (ring)	126.2(4)−128.4(4)		
Mn−O−Mn (center)	126.5(3)−129.7(3)		
		5	
Zn(5)−O(3)	2.312(9)	Zn(5)−N(14)	2.072(9)
Zn(5)−N(41)	2.015(11)	Zn(5)−O(4)	2.084(9)
Zn(5)−O(9)	2.133(10)	Zn(5)−O(10)	2.134(9)
Zn−O	2.084(9)−2.312(9)	Zn−N	1.968(11) − 2.409(12)
Zn−O−Zn (ring)	134.2(5)−137.8(4)		
Zn−O−Zn (center)	133.4(4)−136.6(4)		
		6	
Pb(1)−O(1)	2.459(5)	Pb(2)−O(2)	2.468(5)
Pb(1)−O(2)	2.497(5)	Pb(2)−O(5)	2.500(5)
Pb(1)−O(4)	2.467(9)	Pb(3)−O(1)	2.498(5)
Pb(3)−O(3)	2.454(5)	Pb(1)−N(5)	2.427(6)
Pb(2)−N(7)	2.350(6)	Pb(2)−N(9)	2.585(5)
Pb(3)−N(1)	2.583(5)	Pb(3)−N(3)	2.348(6)
Pb(1)−O(1)−Pb(3)	128.40(19)		
		7	
Fe(3)−O(3)	2.041(7)	Fe(3)−O(4)	2.020(8)
Fe(3)−O(9)	2.002(8)	Fe(3)−O(10)	1.991(9)
Fe(3)−N(14)	2.081(9)	Fe(3)−N(41)	2.084(9)
Fe−O	1.957(7)−2.041(7)	Fe−N	2.011(8)−2.201(8)

the sides, and *trans*-MnN_2O_4 in the center. Although there is an excellent match between the grid core dimensions and the arrangement of the six tritopic ligands, the five-membered chelate rings that form lead to some strain at the terminal pyridine coordination positions, leading to very long Mn−N distances (2.29−2.42 Å) in the grid plane and highly anisotropic metal sites. The central manganese atom (Mn(5)) is forced into a more tightly bound coordination environment (Mn−L 2.19−2.27 Å). Overall, Mn−N distances are comparable to those observed in **1**, but the terminal pyridine contacts in **1** are somewhat smaller (2.23−2.34 Å).[16] Mn−O distances fall in the range of 2.14−2.27 Å.

The aromatic rings of each ligand are almost eclipsed with their neighboring counterparts. Estimates of separations between the pyridine rings can be obtained from the 4-pyridine carbon distances on the terminal rings (3.50−3.84 Å; average 3.654 Å) and the Cl−Cl separations on the central pyridine rings (3.53−3.90 Å; average 3.742 Å) and suggests some significant interaction between the aromatic π electron clouds. The [3 × 3] square grid can be envisaged as a fusion of four individual [2 × 2] [$M_4(\mu\text{-}O)_4$] square grids, and each square resembles a similar Mn_4 [2 × 2] grid of the ligand poapz (Scheme 1) reported recently.[12] Dimensions within this Mn_4 square correspond closely with those in **3**. Each Mn_4O_4 square within the [3 × 3] grid has a pseudo-boat structure.

$[Mn_9(Cl2poapz\text{-}2H)_6](NO_3)_6\cdot 22H_2O$ (4). Some difficulty was encountered with the refinement of this structure (R1 = 0.112) (Table 1), and several nitrate anions, which are clearly there based on the elemental analysis, were not identified in the model and presumably reside among the lattice components assigned to water molecules. The cationic grid fragment is however clearly defined and appears as a strong molecular ion peak in the MALDI/TOF mass spectrum (vide infra). The structure of **4** is very similar to that of **3**, and a view looking along the Mn_9 pseudo-plane is shown in Figure 2. Again the ligands are roughly eclipsed, but the presence of terminal pyrazine rings on the ligand Cl2poapz, rather than pyridine, leads to some differences in distances and contacts within the grid structure. Mn−Mn distances in the outer ring of eight metals fall in the range of 3.85−3.95 Å (average 3.905 Å), while those involving the central Mn fall in the range of 3.90−3.95 Å (average 3.919 Å), indicating a slight contraction of the Mn_9 internal grid size. Distances between the pyrazine 4-nitrogen atoms in adjacent rings fall in the range of 3.43−3.64 Å (average 3.535 Å), in keeping with this observation, while adjacent Cl−Cl contacts fall in the range of 3.66−4.01 Å (average 3.803 Å), slightly larger than in **3**. Mn−O and Mn−N distances compare closely with those in **3**.

$[Zn_9(2poap\text{-}2H)_3(2poap\text{-}H)_3](NO_3)_9\cdot 24H_2O$ (5). The final level of refinement of this structure (R1 = 0.11) (Table 1) is somewhat marginal, but the nonanuclear cation is clearly defined, and six nitrate groups have been located in the lattice, along with many peaks reasonably assigned to oxygen atoms. However, the elemental analysis suggests that in reality there are nine nitrates in the complex. We assume that at this level of refinement a distinction between clusters

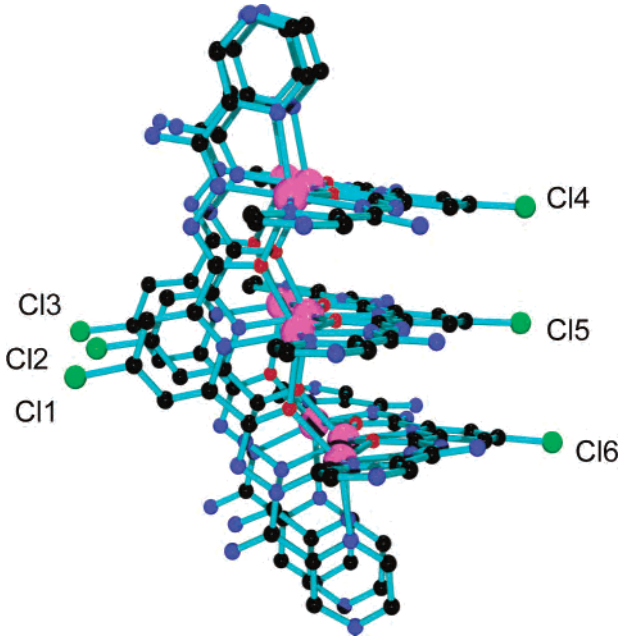

Figure 2. Structural representation of the cation in $[Mn_9(Cl2poapz\text{-}2H)_6](NO_3)_6 \cdot 22H_2O$ (**4**) (carbon = black, nitrogen = blue, oxygen = red, manganese = magenta, and chlorine = green).

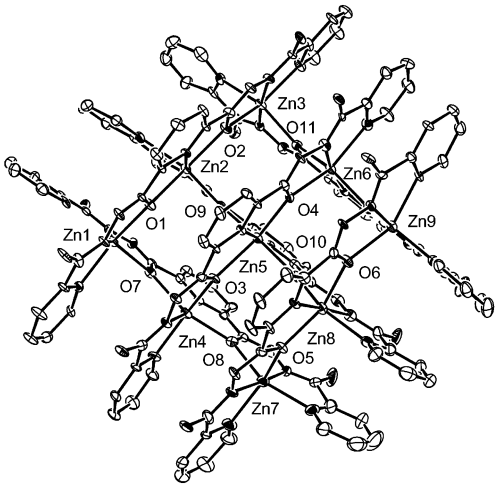

Figure 3. Structural representation of the cation in $[Zn_9(2poap\text{-}2H)_3(2poap\text{-}H)_3](NO_3)_9 \cdot 24H_2O$ (**5**).

of oxygen centers and nitrate groups cannot successfully be made. This assignment indicates that three ligands behave as dianions, while three are monoanionic. The essential features of the structure, as they pertain to the cation, can therefore be reasonably discussed.

The structural representation of the nonanuclear cation is illustrated in Figure 3, and selected bond distance and angle data are listed in Table 2. Nine Zn(II) ions are bridged by 12 alkoxide oxygen atoms, with two groups of three roughly parallel ligands above and below the $[Zn_9(\mu\text{-}O)_{12}]$ plane, in an arrangement essentially identical to that in **1**−**4**. Zn−N bond distances axial to the grid plane are fairly short (1.96−2.05 Å), while in plane contacts to the terminal pyridine rings are much longer (2.11−2.41 Å), in general agreement with trends in the structures of **1**−**4**. Zn−O distances fall in the range of 2.08−2.32 Å, with the longest contact between the central zinc atom Zn(5) and O(3) (2.312(9) Å). The zinc

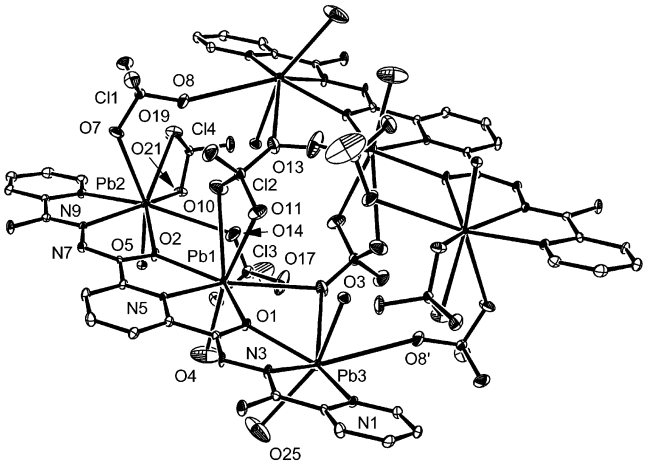

Figure 4. Structural representation of the hexanuclear Pb(II) cluster in $[Pb_3(2poap\text{-}2H)(ClO_4)_4]_2 \cdot 8H_2O$ (**6**).

atoms in the external Zn_8 ring can be considered as roughly tetragonally compressed, while the central zinc atom Zn(5) has one very long contact resulting in an asymmetric axial distortion. Zn−O−Zn angles fall in a fairly narrow range (133.4−137.8°), and Zn−Zn contacts are in the range of 3.908−4.116 Å. The long Zn(4)−Zn(5) distance (4.116(2) Å) is in keeping with the large Zn(5)−O(3) separation (vide supra). These dimensions are slightly larger than those in **1**−**4**. C−O bond distances involving the oxygen bridging atoms fall in the range of 1.27−1.31 Å, indicating the possible presence of some double bond character in some CO groups, but given the present state of refinement little can be concluded, and the two types of ligand cannot really be distinguished.

$[Pb_3(2poap\text{-}2H)(ClO_4)_4]_2 \cdot 8H_2O$ (6). The structural representation of the lead complex **6** is illustrated in Figure 4, and selected bond distance and angle data are listed in Table 2. Compound **6** does not have a grid structure, in contrast to **1**−**5**, and while there are three Pb(II) ions per ligand bound in the three available coordination pockets, the lead ions protrude enough from these pockets because of longer metal−ligand bonds (Pb−N 2.349−2.584 Å; Pb−O 2.459−2.498 Å), such that it is impossible for a grid to form. Three bare lead ions are exposed requiring extra donors, and rather than binding additional grid ligands, which might have been anticipated, each lead atom binds rather loosely to available oxygen donor centers from the perchlorate ions and water molecules, and two subunits join together to form a hexanuclear dimer. The longest contact shown in Figure 4 is 3.198 Å (Pb(3)′−O(8)). All eight perchlorates are involved in the dimeric association, with several different coordination modes. Perchlorate $Cl(1)O_4$ bridges Pb(2) and Pb(3)′ in a μ_2 fashion, perchlorate $Cl(4)O_4$ acts in a chelating bidentate fashion bonded to Pb(2), perchlorate $Cl(3)O_4$ appears to behave in a monodentate fashion bonded to Pb(2), and perchlorate $Cl(2)O_4$ displays remarkable behavior by acting both as a chelating bidentate and as a μ_2-O bridging bidentate ligand, connecting Pb(1) and Pb(3) with their dimeric counterparts. Water molecules are bound in axial positions to all three metal centers. Pb(1) and Pb(3) are seven-coordinate, while Pb(2) appears to be eight-coordinate. Pb−

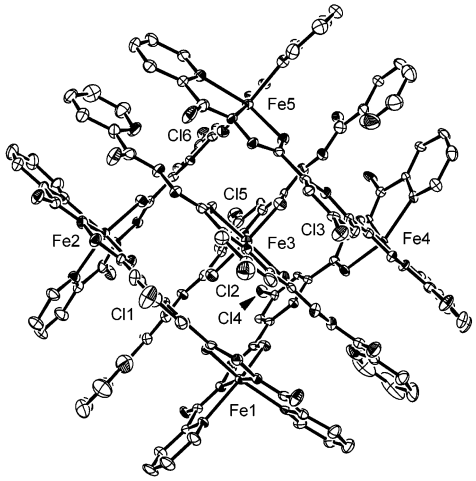

Figure 5. Structural representation of the pentanuclear cation in $[Fe_5(Cl2poap\text{-}H)_6](ClO_4)_9 \cdot 34.5H_2O$ (**7**).

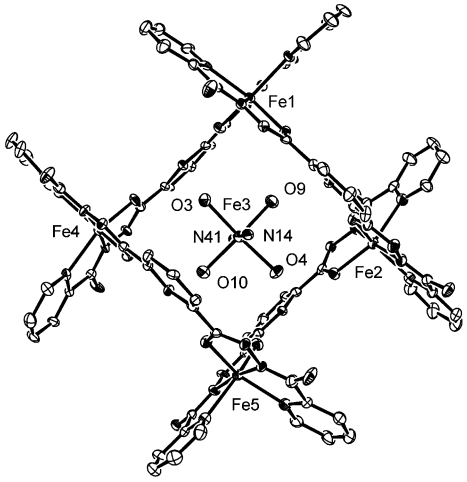

Figure 6. Simplified structural view of the cation in **7** revealing the isolated central Fe(III) center.

Pb distances (Pb(1)−Pb(2) 4.446 Å, Pb(1)−Pb(3) 4.463 Å) are much longer than M−M distances in **1**−**5**, while Pb−O−Pb angles (127.1, 128.4°) compare closely with those in **1**−**5**.

$[Fe_5(Cl2poap\text{-}H)_6](ClO_4)_9 \cdot 34.5H_2O$ (7). As in the case of **4** and **5**, the refinement of the structure of **7** had some problems (R1 = 0.114), but the pentanuclear cation is however clearly defined and is illustrated in Figure 5. Selected bond distance and angle data are listed in Table 2. Figure 6 shows a simplified structure, with the completely isolated central metal ion highlighted without the two N_2O tridentate ligands. What is immediately striking about the structure is the gridlike arrangement of six ligands, in two parallel groups of three, above and below a planar array of just five pseudo-octahedral Fe(III) metal ions. The metal ions are arranged with four at the corners of a large square and one in the middle, with empty coordination pockets in between. The obvious result of this arrangement is that the $[Fe(3)(Cl2poap)_2]$ central fragment appears to be held in place by what are just electrostatic forces. There is no evidence to indicate, for example, water molecules in the empty sites. Edge Fe−Fe distances fall in the range of 7.82−7.87 Å, while distances from Fe(3) to the corner iron centers fall in the range of 5.37−5.71 Å. Nine perchlorate anions show up clearly in the lattice structure, indicating that each ligand has lost one proton on average. In other related M_9 grid structures (e.g., **1**−**5**), the metal sites comprise three different types: (a) a central *trans*-M_2O_4, (b) four corner *cis*-MN_4O_2, and (c) four side *mer*-MN_3O_3 centers. In **7**, the central and corner Fe(III) centers are present, but the *mer*-MN_3O_3 sites are unoccupied. If the overall structure is considered in terms of the five metals drawing the six ligands into the grid arrangement, an examination of metal−ligand distances and the size of the empty sites might reveal some reason as to why a fully metalated grid is not formed.

The central metal (Fe(3)) has relatively short Fe−ligand bond distances (1.991−2.084 Å) typical for Fe(III), with a somewhat distorted *trans*-FeN_2O_4 octahedral geometry. The corner FeN_4O_2 iron centers (Fe(1), Fe(2), Fe(4), and Fe(5)) have much more distorted six-coordinate geometries, with two quite long Fe−N contacts (2.150−2.201 Å) and much shorter remaining bonds. The long bonds, without exception, are those involving terminal pyridine donors. A similar situation occurs in **3**−**5** but with generally longer contacts consistent with the M(II) oxidation state. This suggests a certain amount of strain in the structure as the ligands span the metal grid arrangement. The size of the empty side coordination pockets can be estimated from the distances between the trans atoms that would form the octahedral site (e.g., O(11)−O(12) 4.402 Å, N(16)−N(50) 4.138 Å, and O(4)−N(18) 4.363 Å), and halving these would give an estimate of potential Fe−ligand distances. Such large separations would not be typical for a single Fe(III) ion, and this suggests that these sites may not be attractive to Fe(III). Another significant feature is the 4-chlorine atom on the central ligand pyridine ring, which would exert an electron-withdrawing effect within this ring, thus rendering this nitrogen donor site less basic. In this context, the fact that the only Cl-substituted pyridines that coordinate are those binding to the central iron Fe(3) is significant (vide infra). In other respects, the incompletely metalated grid resembles the typical M_9 grids, with essentially parallel arrangements of ligands with typical separations between the aromatic rings in the range of 3.6−4.1 Å.

The extended lattice structure in **7** is quite complex but shows that the grids are arranged in a columnar fashion along the *x* axis (Figure 7; only Fe and oxygen centers are shown, and for convenience some oxygen atoms have been linked to highlight the Fe_5 subunits). The shortest Fe−Fe distance along the columns is 12.60 Å (Fe(1)−Fe(4)), while between columns in the layers in the *y* axis direction the shortest distance is 9.87 Å (Fe(2)−Fe(4)). Such long Fe−Fe distances within the columns and along the layers are not considered of significance in terms of intermolecular magnetic superexchange interactions (vide infra).

Mass Spectral Studies. The problematic nature of structural solutions with large molecules of this type prompted us to look for other physical evidence for grid formation and a quick method for the screening of products. MALDI/TOF mass spectra have been useful in some cases, and for **2**−**4** molecular ions were observed in positive ion mode.

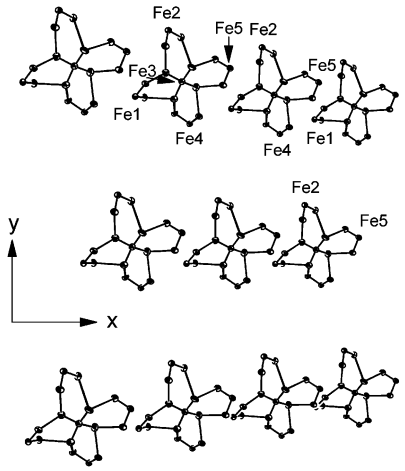

Figure 7. Lattice structural projection of **7**. Some O−O bonds are joined to highlight the five Fe(III) centers as a single unit.

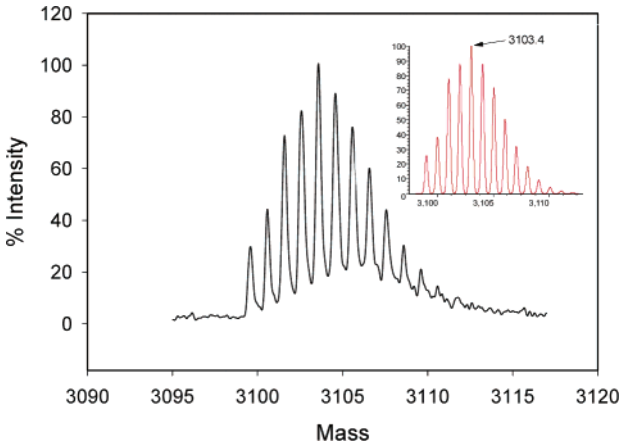

Figure 8. MALDI/TOF mass spectrum for **4** with calculated isotope splitting pattern for the molecular ion.

Figure 8 shows the molecular ion peak for **3** corresponding to M^+ and the simulated spectrum, showing good agreement. Other weaker peaks at higher mass (3203.2, 3305.2) correspond to the molecular grid plus one and two perchloric acid molecules, respectively. Compound **4** showed the correct nonanuclear molecular ion at mass 3113.9. Molecular ions could not be observed for the other compounds, but sensible fragments were observed.

Self-Assembly Reactions. The high yield self-assembly reactions involving tritopic ligands such as 2poap, Cl2poap, Cl2poapz, and 2poapz to produce grid structures is well-demonstrated with a variety of transition metal salts, despite the excess of metal salts that is generally used in the reactions, which might favor, for example, trinuclear derivatives. Structural proof of the [3 × 3] nonanuclear grid structures has been limited so far to the manganese(II), copper(II), and zinc(II) cases, in large measure because of difficulties in obtaining suitable stable crystals. In the Mn(II) cases each ligand loses two protons, but for Cu(II) only one proton is lost per ligand, and with Zn(II) it appears that in the case of **5** three ligands lose one proton and three ligands lose two (vide supra). Bond distances within the ligands do not reveal clearly the sites of ligand deprotonation. In other cases cobalt(II), nickel(II), and iron(III) salts have been shown to form similar systems.[20] The self-assembly can be attributed to the excellent matching of the coordination site pockets of the ligands, which provide six judiciously positioned donor atoms per metal and the requirements of the nine pseudo-octahedral metal ion centers in the grid structure. A significant factor in the parallel docking of the two groups of three ligands above and below the M_9 plane must be the proximity of the aromatic π electron clouds on the pyridine and pyrazine rings, as indicated by the relatively short distances between these aromatic rings (~4 Å; Cl−Cl separations in **3** and **4** fall in the range of 3.5−4.0 Å). These interactions would presumably be repulsive in nature in general.[27]

The prominence of the self-assembly processes and high yields of the M_9 grid complexes indicates the minimal occurrence of oligomeric species and other unrelated complexes in the reaction mixtures. However, in the reaction between $Ni(BF_4)_2 \cdot 6H_2O$ and 2poapz, a dinuclear helicate complex $[Ni_2(poapz)_3F)](BF_4)_3 \cdot 8.5H_2O$[28] was obtained in low yield (12%). In this structure, a hydrogen bonded fluoride ion occupies a central cavity created by three spirally oriented ligands. This has no structural connection to the self-assembly process and the ultimate grid structure and appears to be a simple spiral assembly product, the formation of which is driven by the unusual hydrogen bonding arrangement in the central cavity, the hydrolytic instability of BF_4^- producing F^-, and the slightly acidic reaction conditions. This type of complex is not uncommon with flexible bis-bidentate ligands with well-separated coordination compartments. The other product in the reaction between 2poapz and $Ni(BF_4)_2$ was found to be the expected Ni_9 [3 × 3] grid, which exhibited intramolecular antiferromagnetic coupling.[20] Copper is perhaps an unusual case since it has a preference for five-coordination rather than six, and in one case an octanuclear Cu_8 cluster is formed with a central core of four six-coordinate Cu(II) centers and four five-coordinate centers arranged in a pinwheel fashion outside the core.[29] One clear exception to the general trend of M_9 grid formation is **7,** where a most unusual incomplete pentanuclear grid structure is formed.

The apparent preference of the pentanuclear open-grid in **7**, even in the presence of weak base, can be viewed in terms of an assembly process in which a square [2 × 2] grid involving four well-separated ligands, and the corner metal centers could possibly form first. These Fe(III) atoms would then avoid the more weakly donating central, chloro-substituted pyridine rings. The insertion of the central Fe(III) unit into the grid could then occur via precoordination of an Fe(III) atom to the central NO_2 pocket of one additional ligand with, for example, solvent molecules filling remaining coordination sites, which then slides between two ligands in the square grid to be met by an approaching ligand on the other side. Possible attractions between electron-poor

(27) Hunter, C. A.; Sanders, J. K. M. *J. Am. Chem. Soc.* **1990**, *112*, 5525.
(28) Thompson, L. K.; Matthews, C. J.; Zhao, L.; Wilson, C.; Leech, M. A.; Howard, J. A. K. *J. Chem. Soc., Dalton Trans.* **2001**, 2258.
(29) Xu, Z.; Thompson, L. K.; Miller, D. O. *J. Chem. Soc., Chem. Commun.* **2001**, 1170.

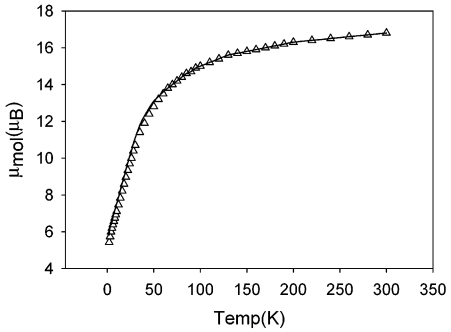

Figure 9. Magnetic data (μ_{mol} vs T) for $[Mn_9(Cl2poap\text{-}2H)_6](ClO_4)_6 \cdot 10H_2O$ (**3**). The solid line corresponds to a fit to eq 1, with $g = 2.0$, $J1 = -4.6$ cm^{-1}, and $J2 = 0$ cm^{-1}.

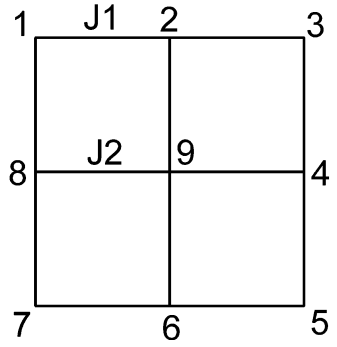

Figure 10. Magnetic exchange model for a $[M_9(\mu\text{-}O)_{12}]$ grid.

coordinated pyridine rings bonded to the corner Fe(III) centers and terminal, uncoordinated, more electron-rich uncoordinated pyridine rings of the central fragment could well facilitate this process.[27]

1, 3−**5**, and **7** are not subject to crystal-field stabilization effects and so are somewhat plastic within the confines of the nine coordination pockets produced by the assembly of six ligands. Stereochemical distortions at the metal centers are therefore considered to be somewhat random and subject to packing forces and the constraints of the ligand itself. For $[Cu_9(2poap\text{-}H)_6](NO_3)_{12} \cdot 9H_2O$ (**1**), where the copper(II) ion is subject to crystal-field effects, Jahn−Teller distortion, and possibly the ligand charge, the copper centers are highly distorted. In the grid all the metal ions appear to have enough room within the coordination pockets to seek preferred orientations in which their magnetic planes end up in orthogonal arrangements throughout the grid, leading to a combination of antiferromagnetic and ferromagnetic behavior, with ferromagnetic coupling dominating at low temperatures and a $S = 7/2$ ground state.[17,18,20]

Magnetic Properties. 1, 3, and **4** have very similar magnetic properties, and a plot of μ_{mol} versus T for **3** is illustrated in Figure 9. The moment drops from 16.8 to 5.7 μ_B at 2 K. This behavior is consistent with the presence of significant antiferromagnetic coupling within the grid, with a low-temperature moment that is equivalent to one uncoupled Mn(II) center. The room-temperature moment is consistent with the presence of nine high-spin Mn(II) centers, but the low-temperature value points toward a $S = 5/2$ ground state. Magnetization data as a function of field at 1.8 K confirm this for **1**,[19] with a good fit to the appropriate Brillouin function for a $S = 5/2$ spin system in the range of 0−3 T. An isotropic exchange model for this type of grid (eq 1; Figure 10) should include

$$H_{ex} = -J1\{S_1 \cdot S_2 + S_2 \cdot S_3 + S_3 \cdot S_4 + S_4 \cdot S_5 + S_5 \cdot S_6 + S_6 \cdot S_7 + S_7 \cdot S_8 + S_1 \cdot S_8\} - J2\{S_2 \cdot S_9 + S_4 \cdot S_9 + S_6 \cdot S_6 + S_8 \cdot S_9\} \quad (1)$$

two exchange integrals, and a full-exchange Hamiltonian should also include dipole−dipole terms, second-order ligand field terms, and Zeeman terms. Such an analysis is impeded by the enormous dimensions of such a calculation and even in employing spin rotational and D_4 spin permutational symmetry, the calculations exceed most computer capabilities.[19,30] To simplify the exchange situation, the grid can be considered as the sum of a ring of eight Mn(II) centers (1−8; Figure 10) coupled to the central Mn(II) ion (9; Figure 10). Since the magnetic properties of the system are clearly dominated by antiferromagnetic exchange and since the ground state appears to be $S = 5/2$, it is reasonable to assume that $J1$ is negative and dominates the exchange situation and that $|J1| > |J2|$. The data for **1** have been successfully fitted to an isotropic exchange model based on Figure 10, with $g = 2.0$, $J1 = -3.8$ cm^{-1}, and $J2 = 0$ cm^{-1}.[19] Similar fits for **3** and **4** gave $g = 2.0$, $J1 = -4.6$ cm^{-1}, $J2 = 0$ cm^{-1} and $g = 2.03$, $J1 = -4.1$ cm^{-1}, and $J2 = 0$ cm^{-1}, respectively. The solid line in Figure 9 corresponds to the fitted parameters for **3**. $J1$ values for these compounds are comparable with the exchange integral found for the $[Mn_4(\mu\text{-}O)_4]$ square grid complex $[Mn_4(poapz\text{-}H)_4(H_2O)_4](NO_3)_4 \cdot H_2O$ ($J = -2.85$ cm^{-1}),[12] in keeping with the similar structural elements present in both systems.

The pentanuclear grid (**7**) exhibits rather unremarkable magnetic properties with a profile of $\mu_{(mol)}$ as a function of temperature that is essentially invariant with field (100, 1000 Oe) and drops slightly from 13.2 μ_B at 300 K to 12.2 μ_B at 20 K, followed by a more pronounced drop to 10. 3 μ_B at 2 K. This behavior is reasonably associated with a weak intramolecular antiferromagnetic exchange component, with a possible contribution from zero-field splitting at low temperatures. On the basis of the structure, and the fairly large distances separating individual grids in the lattice, the data were fitted to an isotropic exchange model based on four Fe(III) ($S = 5/2$)

$$H_{ex} = -J\{S_1 \cdot S_2 + S_2 \cdot S_5 + S_4 \cdot S_5 + S_1 \cdot S_4\} + S_3 \quad (2)$$

centers arranged in a square (eq 2; Figure 6), with a single exchange integral and an isolated central Fe(III) center.[31] The fit gave $g_{av} = 2.015$, $J = -0.2$ cm^{-1}, $D = 0$ cm^{-1}, and TIP $= 200 \times 10^{-6}$ emu mol^{-1}. The fit is shown in Figure 11 as

(30) Waldmann, O. *Phys. Rev. B* **2000**, *61*, 6138.

(31) MAGMUN4.0. The data fitting was carried out using an integrated software package that calculates the total spin state combinations and their energies and substitutes them into the van Vleck equation directly within the software. Copies of MAGMUN4.0 are available free of charge through http://www.chem.mun.ca/resinst/. The programs may be used only for scientific purposes, and economic utilization is not allowed. If the routine is used to obtain scientific results that are published, the origin of the program should be quoted.

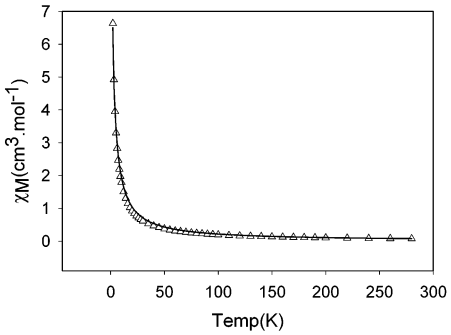

Figure 11. Magnetic data (χ_{mol} vs T) for $[Fe_5(Cl2poap\text{-}H)_6](ClO_4)_9 \cdot 34.5H_2O$ (**7**). The solid line corresponds to the fitted parameters described in the text.

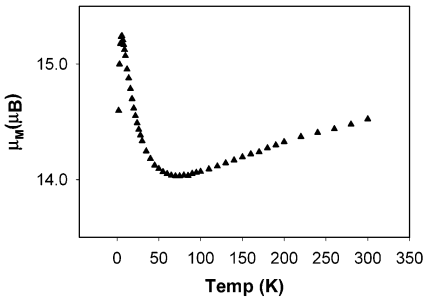

Figure 12. Magnetic data (μ_{mol} vs T) for $[Fe_9(2poap\text{-}2H)_6](NO_3)_{15} \cdot 18H_2O$ (**8**).

a plot of χ_{mol} as a function of temperature (the solid line corresponds to fitted parameters). Inclusion of a zero-field splitting term (D) did not improve the fitting.

A plot of μ_{mol} versus T (Figure 12) for $[Fe_9(2poap\text{-}2H)_6](NO_3)_{15} \cdot 18H_2O$ (**8**) shows a slight drop from 14.5 μ_B at 300 K to a minimum of 14.0 μ_B at 70 K and a steep rise to 15.24 μ_B at 6 K, followed by a slight drop below this temperature. The room temperature moment is significantly lower than that observed for the nominally isoelectronic $Mn(II)_9$ systems (17.8 μ_B for the spin only case for nine $S = 5/2$ centers). The general shape of the profile suggests that intramolecular antiferromagnetic exchange dominates above 70 K, but below 70 K a weaker ferromagnetic component exists in keeping with the rise in moment. Below 6 K the drop in moment could be attributed to an additional antiferromagnetic component or zero-field splitting. A similar general profile is observed for **2**, the Cu_9 system, and has been rationalized in this case in terms of a combination of intramolecular antiferromagnetic and ferromagnetic coupling.[17,18,20] A magnetization versus field profile at 2 K (Figure 13) shows that M rises to a large value (27 Nβ), but the system is not saturated at 5 T, and comparison with standard Brillouin functions indicates that the compound does not behave as a magnetically coupled high-spin ground state system. Interestingly, the M/H data can be successfully fitted to the summed Brillouin functions for an assembly of nine essentially independent $S = 3/2$ centers ($g = 2.04$, $T = 2$ K), suggesting that at 2 K each Fe(III) center has a resultant spin associated with three unpaired electrons. It is therefore reasonable to suggest that these are the electrons lying in the metal ion t_{2g} orbitals and that the antiferromagnetic interactions are localized in the e_g orbitals only.

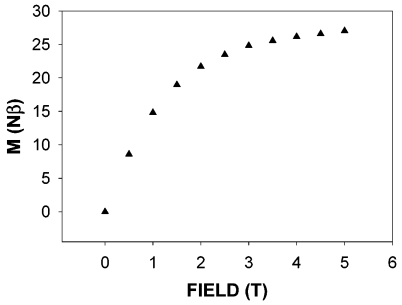

Figure 13. Magnetization (M/H) data for $[Fe_9(2poap\text{-}2H)_6](NO_3)_{15} \cdot 18H_2O$ (**8**) at 2 K.

The magnetic properties of **8** are quite different from **1**, **3**, and **4**, despite the fact that all systems nominally have nine $S = 5/2$ metal ions. In the absence of a structure on **8** it is difficult to make a fully informed assessment of the exchange situation, but it is clear that nine high-spin Fe(III) centers are present (vide infra) in a grid structure. The geometries at each Fe(III) center are likely to be quite different from the Mn(II) centers in **1**, **3**, and **4**, associated in part with the different ionic charge. The M−O−M bridge angles are also likely to be somewhat different in the iron system but will of necessity be large and consequently should lead to antiferromagnetic exchange terms, which can be associated with the drop in μ_{mol} from 300 to 75 K. We await a structure on this system to more fully evaluate the unusual magnetic properties.

Mössbauer Spectroscopy. Low-temperature Mössbauer spectroscopy data (77 K, Figure 14a) have however provided indirect structural evidence for the presence of three groups of different Fe(III) centers with the intensity ratio 1:4:4, consistent with the proposed Fe_9 grid structure and the stoichiometry indicated by the chemical analysis of **8**. The quadrupole splittings corresponding to Figure 14 are 0.58 mm/s (3,4), 1.05 mm/s (2,5), and 1.86 mm/s (1,6) with the isomers shifts (77 K) all ∼0.5 mm/s relative to iron metal and typical of high-spin Fe(III). The splitting values are indicative[32] of high-spin Fe(III) in a range of distorted six-coordinate environments with the smallest value corresponding to the central Fe atom of the [3 × 3] grid. The latter site exhibits the least distortion in the context of the crystallographically characterized M_9 systems.

On further cooling to 4.17 K (Figure 14b), the spectrum changes, and one sees a strong, rapidly relaxing paramagnetic doublet superimposed on a broad poorly defined hyperfine background pattern for which the average internal field H_n is ∼49.4 T. The latter value of H_n is consistent with $S = 5/2$ Fe(III) in the Fe_9 cluster. (Note that the Lorentzians of Figure 14b are given merely as a guide to the reader. The spectral transitions are not sufficiently resolved so as to allow for a definitive fit, although the overlap of two Zeeman patterns is evident in the raw data.)[32] The overall behavior is consistent with slow paramagnetic relaxation owing to lengthening cluster magnetization reversal times. However, in view of the presence of a rapidly relaxing fraction, the

(32) Greenwood, N. N.; Gibb, T. C. *Mössbauer Spectroscopy*; Chapman and Hall: London, 1971.

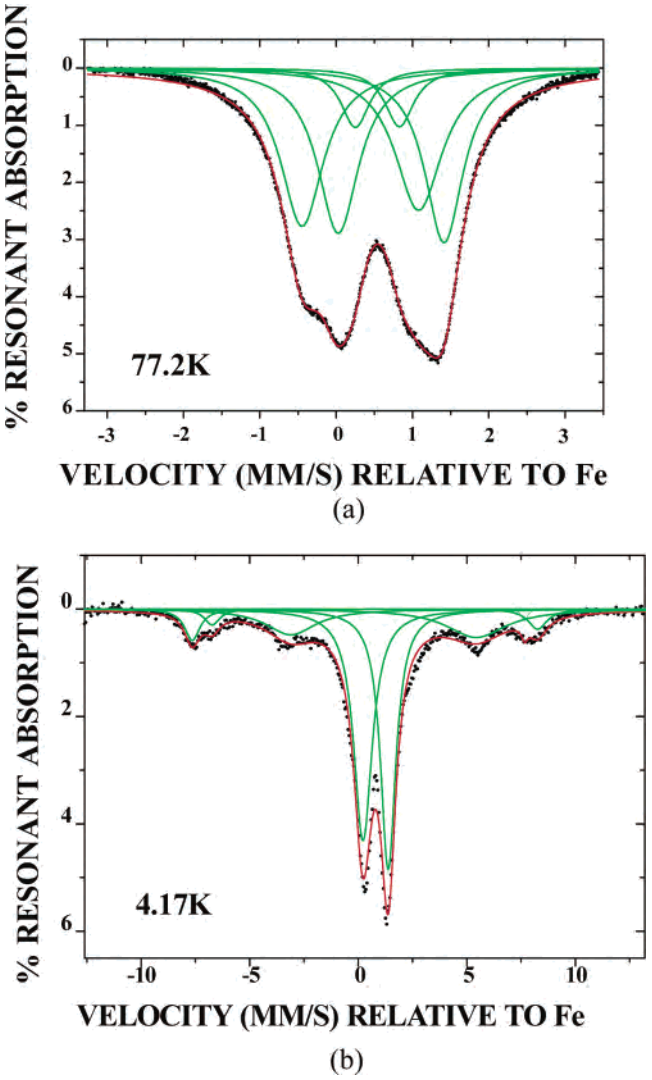

Figure 14. Mössbauer data for $[Fe_9(2poap\text{-}2H)_6](NO_3)_{15}\cdot 18H_2O$ (**8**) at 77.2 and 4.17 K.

system is clearly not yet at the infinitely slow relaxation limit[33] at these temperatures, in contrast to clusters such as Fe_8[34] at 4.2 K or Fe_4[35,36] at 1.3 K. Further very low-temperature *M* versus *H* (hysteresis) studies will be necessary to confirm the possibility of quantum tunneling of magnetization in this and the related manganese analogues.

Mössbauer spectra for the Fe_5 complex (**7**) at ambient temperature, 77 and 4.2 K, are shown in Figure 15. It is immediately obvious that while two sites (the central Fe(3) and four equivalent corner atoms Fe(1), Fe(2), Fe(4), and Fe(5) of Figure 6) are resolved, the percent effect is relatively small. This occurs despite the fact that the room temperature spectrum corresponds to a baseline of some 14×10^6 counts for a compound containing some ~7 wt % Fe. In an attempt to enhance spectral resolution for both the Fe_5 and the Fe_9

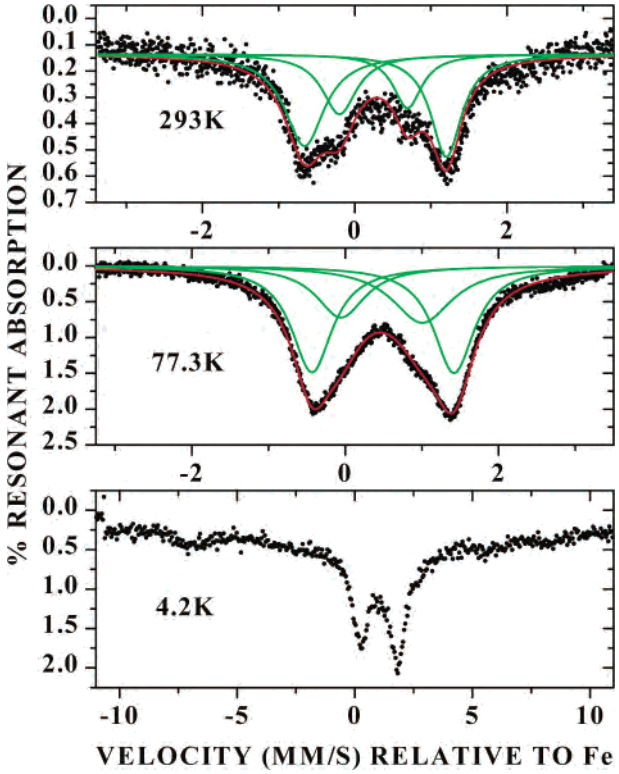

Figure 15. Mössbauer data for $[Fe_5(Cl2poap\text{-}H)_6](ClO_4)_9\cdot 34.5H_2O$ (**7**) at 293, 77.3, and 4.2 K.

complexes, 1024 channels of memory/spectrum were used versus the more typical 512 channels. In this case the signal/noise is somewhat improved at 77 K, although the two doublets are now more highly overlapped at this temperature. The isomer shifts (293 K) for Fe(3) and the corner iron atoms are 0.25 and 0.27 mm/s, respectively, again confirming high-spin Fe(III). The rather large quadrupole doublet (1.86 mm/s) corresponds to the more distorted corner sites (vide ante, X-ray discussion), while the less distorted central atom (Fe-(3)) doublet has a splitting value of 0.89 mm/s.

If the recoil free fractions (*f*) for the corner and central iron atom sites of **7** were equal, one would expect that the intensity ratio *I*(corner)/*I*(central) would be ~4:1. The observed value of this ratio (~2) is substantially less. This is consistent with somewhat weaker local bonding (also suggested by the X-ray data) for corner sites versus the central Fe atom of the grids and other things being equal, a recoil free fraction for corner sites only ~0.5 times that at the center. We speculate that a more global effect may also be operative. That is, with the loss of edge metal atoms on going from the $M_9 \rightarrow M_5$ grid and concomitant reduction of the overall cluster rigidity, there is enhancement of differential recoil free fraction effects.

Finally, it should be noted that the spectrum of **7** at 4.2 K also indicates incipient slow paramagnetic relaxation with a weak hyperfine background pattern. A rough estimate of the internal hyperfine field of the background Zeeman pattern is 48 T, again clearly consistent[32] with high-spin Fe(III). This pattern is somewhat less intense than that observed for the Fe_9 complex, suggesting a smaller ground-state spin and *D* value for the Fe_5 cluster and thus a lower blocking temper-

(33) Wickman, H. H.; Klein, M. P.; Shirley, D. A. *Phys. Rev.* **1966**, *152*, 345.
(34) Barra, A. L.; Debrunner, P.; Gatteschi, D.; Schultz, C. E.; Sessoli, R. *Europhys. Lett.* **1996**, *35*, 133.
(35) Caneschi, A., Cianchi, L.; Del Gaillo, F.; Gatteschi, D.; Moretti, P.; Pieralli, F.; Spina, G. *J. Phys.: Condens. Matter*. **1999**, *11*, 3395.
(36) Cianchi, L.; Reiff, W. M.; Caneschi, A.; Del Gaillo, F. *Phys. Rev. B* **2002**, *65*, 064415−1.

ature for superparamagnetic relaxation. However, definitive comments on this point await a detailed investigation of the frequency dependence of χ'(ac) and χ''(ac) over the range of 1.5 K (or preferably lower) to 20 K.

Conclusions

Aromatic polytopic ligands, with a contiguous linear arrangement of coordination pockets and alkoxide groups in adjacent sites, readily self-assemble with Mn(II), Cu(II), and Zn(II) salts to produce nonanuclear [3 × 3] grid structures, with the ligands arranged in parallel groups of three above and below the metal plane. Spectroscopic and other evidence indicate that similar grids are produced with Ni(II), Co(II), and Fe(III). The Pb(II) complex, with a trinuclear subunit structure, clearly indicates that the metal ion radius is an important factor in the self-assembly outcome and that despite the large coordination pocket sizes observed in the M_9 systems in general, large cations such as Pb(II) cannot be accommodated in a gridlike arrangement. The unusual remote Fe_5 grid (**7**) is anomalous within the group and clearly indicates that there are subtle features of these systems that require further exploration.

The present class of grids is the first type of self-assembled [3 × 3] grid system to incorporate paramagnetic metal centers with short-range bridging connections and the presence of intramolecular spin−spin exchange interactions. Antiferromagnetic coupling occurs for all of the systems, in agreement with the presence of M−O−M bridges with large (125−135°) bridge angles and direct magnetic orbital overlap, but magnetic orbital orthogonality in the copper(II) case leads to ferromagnetic exchange as well. The Fe(III) grid appears to behave in a somewhat similar fashion. External dimensions of the grid cationic fragments are of the order of 20 × 20 Å, which is attractive for possible information storage. An assembly of close-packed grids in a two-dimensional array, with one data bit (B) stored per grid, would lead to a potential surface data storage density of ∼160 TB/in^2, an attractive figure given the rapidly approaching upper limits with conventional magnetic data storage media resulting from thermal erasure at the superparamagnetic limit.

This type of ligand can be readily modified to include external sulfur bearing groups (e.g., Scheme 1, R′ = S^-, RS^-), and given the unrestricted external projection of the chlorine atoms in **3** and **4**, molecular deposition on, for example, a gold surface is a realistic proposition. Preliminary surface deposition experiments on flat gold surfaces have been carried out from dilute acetonitrile solutions of Mn(II)$_9$ grid complexes of, for example, R2poap (R = S^-). Close-packed monolayers have been successfully produced and probed using STM techniques,[37] and individual molecular dimensions are found to be of the order of 2.6 nm.

Acknowledgment. We thank the Natural Sciences and Engineering Research Council of Canada (NSERC) for financial support and Dr. R. McDonald and Dr. M. J. Ferguson (University of Alberta) for structural data. Dr. O. Waldmann (University of Erlangen) is thanked for assistance with magnetic calculations on compound **3**.

Supporting Information Available: X-ray crystallographic data in CIF format for **3**−**7**. This material is available free of charge via the Internet at http://pubs.acs.org.

IC020468Y

(37) Shapter, J.; Weeks, L.; Thompson, L. K. Unpublished results.